Applied Water Science (2023) 13:234
https://doi.org/10.1007/s13201-023-02033-x

ORIGINAL ARTICLE

Geophysical assessment of seawater intrusion: the Volturno Coastal Plain case study

D. Tarallo[1] · I. Alberico[2] · G. Cavuoto[1] · N. Pelosi[1] · M. Punzo[1] · V. Di Fiore[1]

Received: 25 May 2023 / Accepted: 13 October 2023 / Published online: 14 November 2023

Abstract
In coastal alluvial plains, the variability of sedimentary inputs, tectonic and eustatism causes a complex subsurface geology which influences the position of fresh/saltwater interface. Furthermore, in these areas densely populated, the over-pumping of freshwater, coupled with the climate change events, promotes the landward migration of freshwater/saltwater boundary. This research illustrates the ability of geophysical tools to recognize the presence of salt/brackish water at Volturno Coastal Plain, Southern Italy. This area is characterized by a peculiar geological setting, due to the proximity at Somma–Vesuvio and Campi Flegrei volcanic areas, which profoundly influences the circulation of groundwater. The subsurface is mainly characterized by: (i) two denser layers located at − 10 m and − 20 m depth which in part prevents the vertical migration of groundwater, (ii) facies heteropy that facilitates the hydraulic connection between the different geological bodies, (iii) a discontinuous *Campanian Ignimbrite* deposits which favor the hydraulic connection between deeper and shallower aquifers. In this geological framework, 2D-ERT and 3D-ERT integrated with Downhole, Multichannel Analysis of Surface Waves and boreholes made possible to recognize the presence of two main zones with salt and brackish waters, respectively. The first zone, characterized by very low resistivity (≤ 1 Ωm) typical of salt water, stretches 1.5 km inland from the coast. The second zone, with a resistivity between 2 and 5 Ωm typical of brackish water, continues for other 3 km inland. This knowledge is useful for the engagement of all stakeholders (farmers, ranchers and policy makers) in the sustainable use of fresh water and for making water management plan operational tools.

Keywords 2D-ERT · MASW · Downhole · Boreholes · GIS analysis · Integrated approach

Introduction

In the last decades, a common problem of coastal aquifers is the saltwater intrusion, which is the landward migration of freshwater/seawater boundary. The over-pumping of groundwater as well as geological heterogeneity of coastal aquifer, relative sea-level rise and coastal erosion (Ketabchi et al. 2016; Salaj et al. 2018; Meyer et al. 2019) are the main causes of this event. It can also be promoted by the presence of canals as well as other anthropogenic works, that have altered the landscape (Herbert et al. 2015), and natural subsidence related to soil oxidation (Doyle et al. 2007; Manda et al. 2014; White and Kaplan 2017).

The Mediterranean coastal zone, one of most densely populated areas in the world, is exposed to the groundwater over-exploitation (Scheidleger et al. 2004; Doll 2009; Leduc et al. 2017; Mastrocicco and Colombani 2021) and hence to the saltwater intrusion. This problem typifies several Italian coastal plains (e.g., Sardinia, Catania, Tiber, Versilia, Po) (Antonellini et al. 2008 and reference therein) where the lack of sufficient and good quality of water could also cause a reduction in fertile land and biodiversity (Zdruli 2012; Zahangeer et al. 2012; Herbert et al. 2015; Alfarrah and Walraevens 2018; Bhattachan et al. 2018).

The process of saltwater intrusion can be studied with direct and indirect methods. The first method includes the realisation of groundwater salinity profiles and groundwater sampling from monitoring wells (Kim et al. 2018 and reference therein; Jasechko et al. 2020 and reference therein). From these point measurements, the spatial complexity of

✉ I. Alberico
ines.alberico@cnr.it

1 ISPC - CNR, Institute of Heritage Science, Naples, Italy

2 Istituto di Scienze Marine (ISMAR-CNR), sede di Napoli, Calata Porta di Massa Interno Porto, 80133 Naples, Italy

saltwater dispersion can be captured by using multivariate statistical analyses tools such as factor analysis, principal component and cluster analysis (Kim et al. 2018; Busico et al. 2018; Corniello and Ducci 2014).

Anyway, the results obtained with traditional borehole survey technique reflect 'point' pollution situation. The spatial complexity of saltwater bodies could be achieved in a systematic, more rapid and relatively low-cost monitoring with indirect methods (geophysical approaches), such as the multi-electrode resistivity arrays and Airborne Electromagnetic (AEM) methods. These latter allow to map in detail the saltwater intrusion in both space and time domains (Viezzoli et al. 2010; Himi et al.; 2004, Sang-Ho et al. 2002). Among all, the 2D and 3D Electric Resistivity Tomography (hereafter ERT) gives the good results (Chitea et al 2011; Singh et al. 2013; Al-Sayed and El-Quady 2007; Gemail et al. 2004; Cianflone et al. 2018; Muzzillo et al. 2020; Ekwok et al. 2022).

This paper discussed the key role of 2D and 3D ERT to assess the salt/brackish water ingression in coastal plains. The novelty was the use of ERTs profiles and borehole stratigraphies as two mutually reinforcing types of data suitable to improve the knowledge of subsurface geology and the distribution of salty and/or brackish water in coastal areas. In this regard, geological data (boreholes and geological maps) made it possible to develop a preliminary scheme of the subsurface geology later improved by the spatial distribution and shape of geological bodies showed by the ERT profiles. In turn, the borehole stratigraphies, together with the down-hole and Multichannel Analysis Surface Wave, supported the identification of layers salt or brackish water saturated in ERT profiles. Furthermore, the potentiality of Geographic information System (GIS) was used to records, easily analyze, summarize data and to display results with thematic maps and graphics (Giménez-Forcada 2014; Tomaszkiewicz et al. 2014; Chabaane et al. 2018; Al-Halbouni et al. 2021).

The study area is the Volturno Coastal Plain (VCP); it is located in the northwestern part of the Campania Region (southern Italy). The increasing demand of freshwater for agriculture and buffalo breeding requires knowledge on the fresh water availability and possible contamination by sea water intrusion. As the other deltaic plains, it is the mosaic of sediments testifying past environments and natural events occurred in the whole catchment. During the Last Glacial Maximum (LGM, e.g., 24 to 21 ky BP), the lowering of sea level exposed the coastal plains to river erosion whose valleys were successively buried by post-LGM deposits (Boyd et al. 2006; Dalrymple et al. 2006; Tropeano et al. 2011). The subsurface geology of *VCP* is very peculiar since late Pleistocene its geomorphological evolution was strongly controlled by the emplacement of volcanic deposits erupted by the Campi Flegrei and Somma-Vesuvio volcanoes. This area, which remained natural until the early 1800s, was characterized by four main rivers (Volturno, Savone, Regia Agnena, Clanio) and marshy areas near the coastline (Alberico et al. 2018). In the last century, this territory has been deeply modified by human presence and anthropogenic activities (Alberico et al. 2018; Ruberti et al. 2022) and in particular between the 1950s and 1980s, urban expansion increased by about 80% (Alberico et al. 2017). The land use change occurred in the eighties, characterised mainly by the transformation of agricultural and natural areas into urbanised areas, has deeply impacted on surface runoff, aquifer recharge and groundwater flows. Only in the mid-1980s-early 1990s did the rapid decrease of new settlements (new urbanised area = 0.76%) lead to a certain stability of the coastal system and the achievement of a new balance that we observe today.

This study, which can be reproduced in all coastal plains for which geophysical and geological data are available, is fundamental as it provides the information needed to achieve a balance between availability and consumptions of freshwater within a framework of sustainable management of natural resources.

Geological and hydrogeological setting

The investigated area is the coastal plain close to the Volturno River mouth (northwestern part of Campania Region, Southern Italy). This river is 175 km long and drains an area of about 545 km^2 encompassing the Molise and Campania Regions (Fig. 1). Several geological reconstructions (Ippolito et al. 1973; Aprile and Ortolani 1978; Ortolani and Pagliuca 1986; Cinque et al. 1987; Cinque et al. 2000; Bruno et al. 2000) describe the Campania Plain as a morpho-structural basin developing since Late Pliocene, along the palaeo-Tyrrhenian margin of the Apennines fold-thrust belt.

The Campania Plain is bounded by NW–SE, NE–SW and E–W trending faults. The main extensional event linked to the activity of NE–SW normal faults, active between 700 and 400 ka (Milia et al., 2003), produced half-grabens structures (from northwest to southeast: Volturno River, Patria Lake, Campi Flegrei-Acerra and the Naples Bay basins) (Fig. 1) filled by more than 5 km of Quaternary deposits (Mariani and Prato 1988; Milia et al. 2003, 2013).

Starting from the early Pleistocene, the Campania Plain has recorded the onset of rapid tectonic subsidence and marine sedimentation. From the mid-late Pleistocene, continental deposits and the products of intense explosive eruptions related to the Somma–Vesuvio district and Campi Flegrei volcanic fields took place (De Vivo et al. 2001; Milia et al. 2003; Romano et al. 1994; Cinque et al. 1997). During the Last Glacial sea-level fall, a lowstand condition led to a deep erosional phase testified by a surface carved into mid-late Pleistocene substratum and successively dissected by

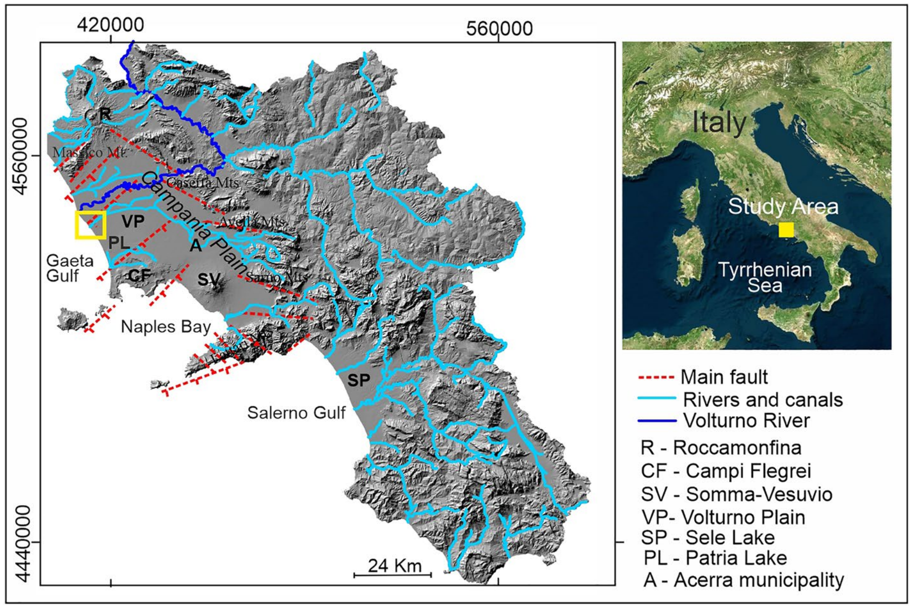

Fig. 1 Location map of the study area at regional (a) and national scale (inset map). The shaded relief shows the landscape morphology, and the yellow rectangle includes the study area

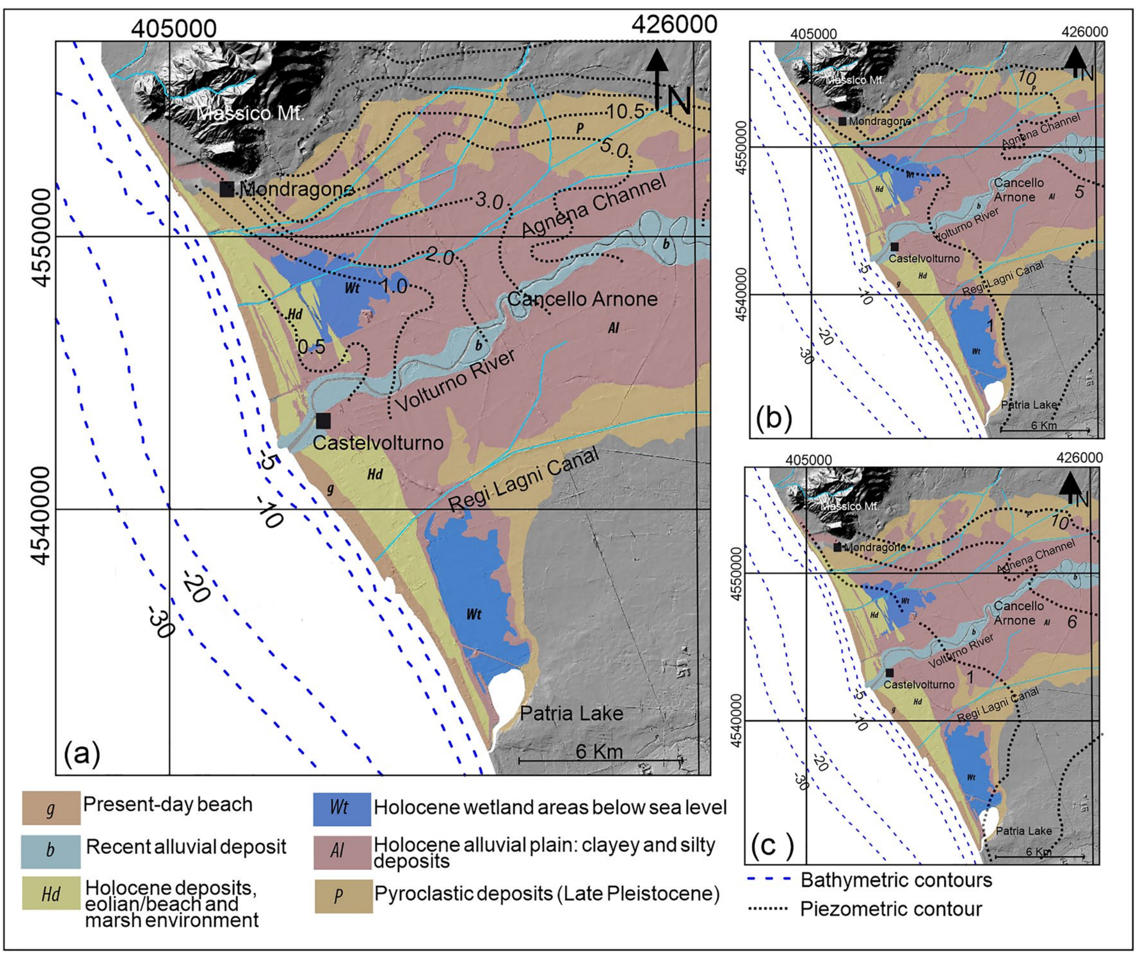

Fig. 2 Simplified geological map (from sheet 171, "Gaeta", 1968-modified) and piezometric contour of main aquifer (from: **a** Corniello et al., (2010), **b** Corniello and Ducci, (2014) and **c** Ducci et al. 2020, modified) overlaid to shaded relief of *Volturno Plain*

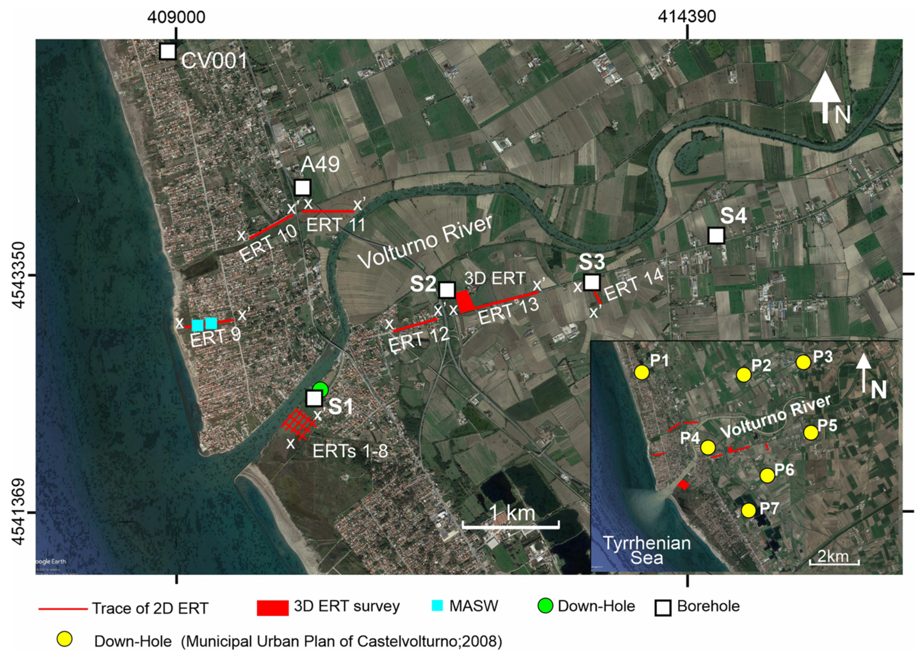

Fig. 3 Location of geophysical survey overlaid to Google Earth image. The red lines are the traces of 2D ERT, the red rectangle evidences the area of 3D ERT survey, the blue light rectangles and the green point identify the location of MASWs and DH, respectively. The white rectangles are the drill-holes. In the inset map, the yellow points represent the DHs realized for the Municipal Urban Plan of Castel Volturno (2008)

Table 1 The number of electrodes, the distance between electrodes and the total investigated length by the single ERT profile are listed

Profile name	Number of electrodes	Distance between electrodes (m)	Total length (m)
Profile 1	48	4	188
Profile 2	48	4	188
Profile 3	48	4	188
Profile 4	48	4	188
Profile 5	48	4	188
Profile 6	48	5	235
Profile 7	48	5	235
Profile 8	48	5	235
Profile 9	96	5	475
Profile 10	96	5	475
Profile 11	96	5	475
Profile 12	96	5	475
Profile 13	96	10	950
Profile 14	96	2.5	475

multiple rivers and buried by the Campania Ignimbrite (CI; 39.85 ± 0.14 ka, Giaccio et al. 2017 and references therein). After this event of rapid vulcanoclastic aggradation, the incision of the plain restarts until reaching the minimum eustatic of 18 ky BP (Siddall et al. 2003; Rohling et al. 2014), which led to an almost complete removal of CI from the valley axis (Romano et al. 1994; Corniello et al. 2010; Amorosi et al. 2012).

The latest Pleistocene-early Holocene sea-level rise promoted the rapid flooding of lower Volturno Plain (Amorosi et al. 2012; Sacchi et al. 2014).

Since ca. 6.5 ky BP, the progressive change from transgressive to regressive conditions marked the establishment of a coastal progradation trend (ca. 4 ky BP). It was testified by the seaward migration of lagoon, beach barrier, alluvial plain and of Volturno River delta (Barra et al. 1989; Cinque et al. 1997; Amorosi et al. 2012) that continues until 1900 (Alberico et al. 2018). Several seismostratigraphic analysis of the outer shelf highlighted the continuity of this structure with a prograding wedge of Falling stage System Tract (late Pleistocene) passing upward to a well-defined Transgressive System Tract and to the Highstand System Track deposits (Iorio et al. 2014; Ferraro et al. 2017). In the plain zone, Plio-Pleistocene pyroclastic, lacustrine, palustrine and marine deposits are overlaid by CI and Holocene alluvial and pyroclastic sediments (Fig. 2). The CI is a gray ashy rock associated with black scoriae and molten lava, with a variable degree of permeability strongly related to the thickness and the physical characteristics (lithification, granulometry, amount of scoria, etc.) that play a key role, as semi-confining or confining bed, in the hydrogeological setting of plain (Corniello and Ducci 2014). It outcrops along the border of Volturno Plain with a thickness of 40–50 m and becomes thinner or absent toward the Volturno River. The main aquifer of the VCP, located in the alluvial, pyroclastic and marine porous sediments underlying the Campanian Ignimbrite, is recharged by the carbonate and volcanic aquifers (Corniello et al. 2010). It is: (i) confined in the areas close to the carbonate reliefs (M.te Massico, M.te Maggiore), where the tufaceous deposits of CI are continuous, (ii) semi-confined in the southern sector of plain and (iii) phreatic near the coast (Corniello and Ducci 2014).

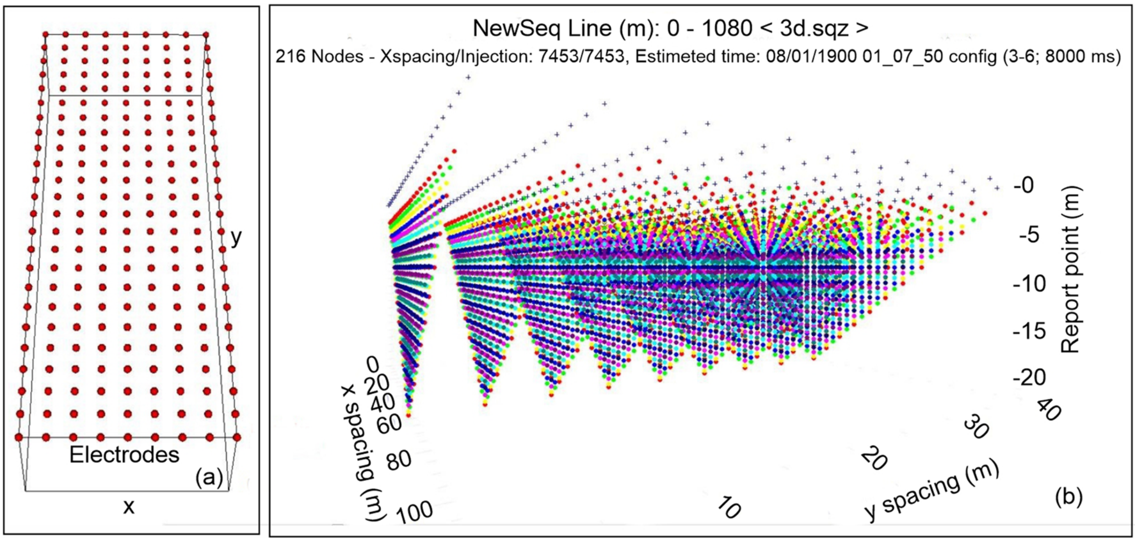

Fig. 4 Geometric field configuration made up of 216 3D electrodes (**a**) and spatial distribution of sampled points (**b**)

A secondary phreatic aquifer occurs in the sand, sand-clay and clay-peat deposits lying on the IC. It is recharged by rainfall infiltration and is then primarily affected by variations in rainfall and temperature. From 2000 to 2018, the rainiest month was November and the driest August. Mean yearly temperature changed from 15.6 °C (years 2005) to 16.8 °C (years 2015 and 2018) and showed an increasing trend of + 0.43° in the period 2000–2019. The hottest months are July and August, while the coldest are December, January and February (Lasagna et al. 2019). Rainfall and temperature together with anthropogenic factors (e.g. high groundwater abstraction), can affect water exchanges, which vary both spatial and temporal domains, between the aquifer and the Volturno River (Celico et al. 2010).

This water echanges can affect the groundwater quality in fact, Corniello et al. (2010) identified high chloride values in the areas close to Volturno River Mouth and along the Volturno River, which has its bed at about − 3.5 m below sea level, and hypotized the intrusion of sea water into the river as far as Cancello Arnone. Busico et al. (2018) evidenced higher value of Na^+ and Cl^- due to seawater intrusion in the area close to the Volturno mouth and only recently, Schiavo et al. (2023) hypothesized that the presence of inland salt water (more than 2 km from the coastline) resulted from trapped palaeowater, rather than actual seawater intrusion, in areas with significant peat layers framed in the subsurface.

In the area close to the Volturno River and in coastal zone, the discontinuity of CI deposits favors the hydraulic continuity between aquifers that become a unique body. The transmissivity ranges from 7.4×10^{-3} to 8.3×10^{-3} m^2/s (Working Group of Water Protection Plan ex Basin Authority of North-Western Campania 2006).

Materials and methods

The analysis of saltwater intrusion at Volturno Plain was realized into two sites: 1) the Volturno coastal zone, dominated by dense urban zones and 2) the rural area located north-eastward of Castel Volturno center, characterized by agricultural lands, sparse farmhouses and few residential buildings (Alberico et al. 2017). For this purpose, 13 2D-ERT (survey date: 2013), 4 3D-ERT profiles (survey dates: May and October 2013 and 2014) were surveyed (Fig. 3).

Furthermore, 2 Multichannel Analysis Surface Wave (MASW), 1 Down-Hole (DH) and 4 new boreholes were acquired to corroborate the interpretation of the ERT profiles (Fig. 3). The shear wave velocity (V_s), compressional waves velocity (V_p) and bulk modulus of 7 DHs (Castel Volturno Municipal Urban Plan 2021), the drill-hole A49 (Caserta Provincial Territorial Plan 2012) and CV001 (Amorosi et al. 2012), closer to the present shoreline, were also considered (Fig. 3).

2D—electrical resistivity tomography

The Wenner–Schlumberger array configuration was adopted for the ERT survey to capture lateral and vertical variations in resistivity of coastal floodplains deposits. Each electrode is both a source of current and a tool to measure electrical potential. This schema is comparable with the horizontal distribution of data points in the pseudo-section of the Wenner array, but it allows to extent of about 10% the investigation depth (Pazdirek and Blaha 1996).

Furthermore, it provides, maintaining the same distance between the electrodes, a better vertical resolution than the

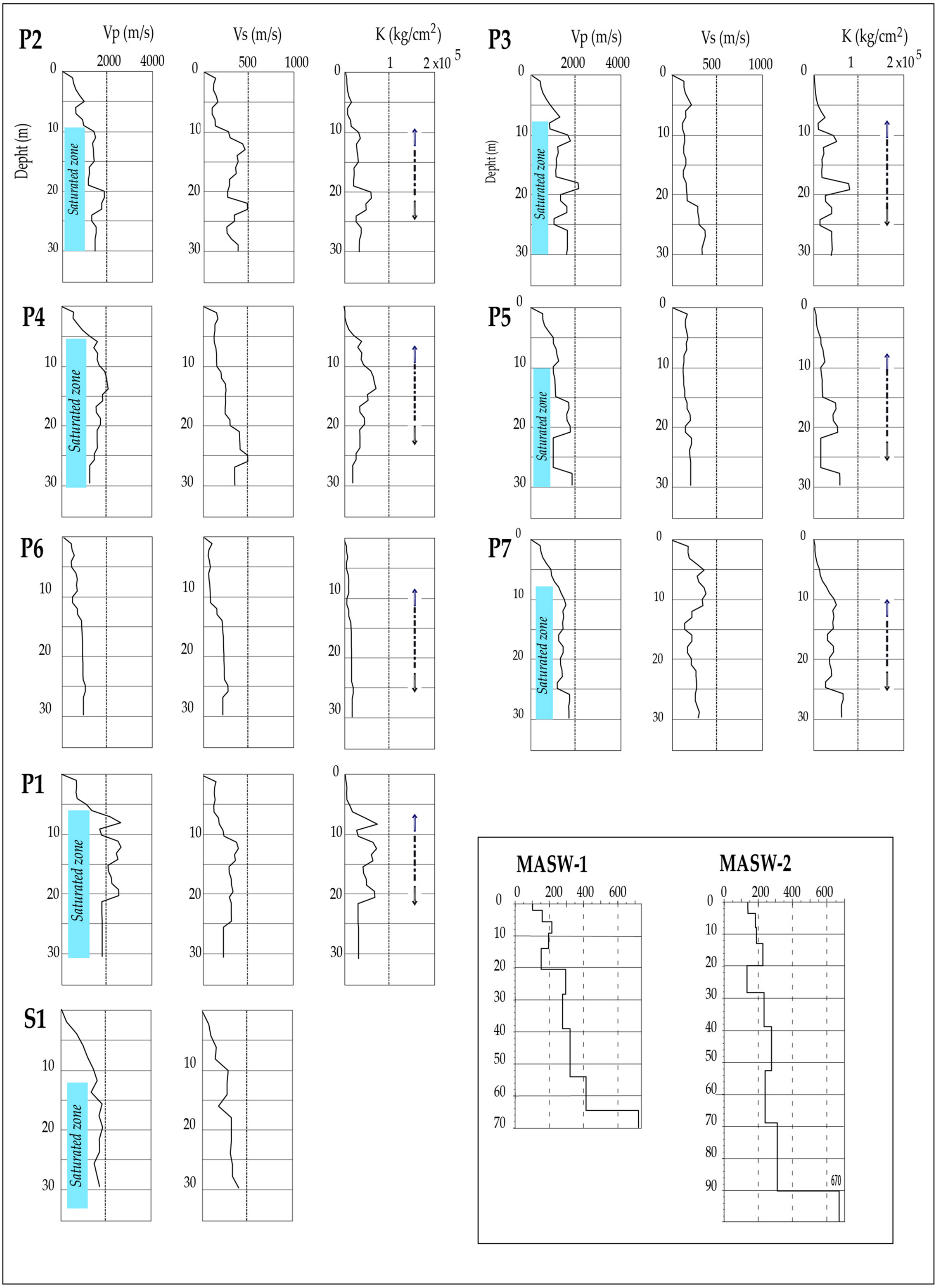

P2
P3
P4
P5
P6
P7
P1
S1
Vp (m/s)
Vs (m/s)
K (kg/cm2)
2000 4000
500 1000
1 2 x10 5
Depht (m)
0
10
20
30
Saturated zone
MASW-1
MASW-2
0 200 400 600
40
50
60
70
80
90
670

◂**Fig. 5** The diagrams display the V_s, V_p and the bulk modulus values plotted versus depth; the light blue color indicates the saturated zone. In the box on the lower right, the V_s versus depth for MASW1 and MASW2 is reported

Schlumberger array. In the coastal zone, 11 *2D ERT* profiles were acquired (Fig. 3). Two systems made up of 48 electrodes spaced 4 m apart and of 96 electrodes spaced 5 m apart were used to survey the profiles from 1 to 8 and from 9 to 11, respectively (Table 1, Fig. 3).

In the rural zone, the 2D ERT profiles from 12 to 14 (Fig. 3) were realized using a system with 96 electrodes. The equidistance between electrodes varied from 5 to 2.5 m (Table 1).

The processing of ERT sections followed a workflow consisting of three main steps: (i) removal of data with an apparent resistivity < 0.01 Ωm and with standard deviation > 5%, (ii) calculation of apparent resistivity pseudo-sections; (iii) data inversion (Loke and Barker 1996a).

3D—electrical resistivity tomography

The 3D *ERT survey* was carried out with the Wenner–Schlumberger array along a cross-diagonal survey to reduce the number of measurements and acquisition time (Loke et al. 2014). The potential measured, over two consecutive years, by electrodes placed on the *x*- and *y*-axes and on 45° lines (Fig. 4a) made it possible to monitor saltwater intrusion in 4D (space–time domain).

The *3D ERT survey* was realized for an area of 4600 m^2. It was divided in a rectangular grid made up of 9 profiles, each of one composed of 24 electrodes (total electrodes, 216) spaced 5 m apart in both x and y directions (Fig. 4b).

The same workflow adopted for the evaluation of 2D resistivity model was also applied to the 3D model. The inversion procedure was based on the smoothness-constrained least-squares routine (Loke and Barker 1996b) that determines with an iteratively method the 3D resistivity model of the subsoil.

Seismic survey (MASW and DH)

MASWs are particularly useful for measuring the V_s of all geological layers within the geophone scheme, while the DH test provides a one-point velocity (V_p and V_s) measurement (Di Fiore et al. 2015, 2020).

The *MASW-01* and *MASW-02* (Fig. 5) were acquired at sites 102 and 200 along the profile *ERT 9* (Fig. 3). The MASW schema is made up of 72 geophones (4.5 Hz) spaced 2 m apart, a seismic source (striking Hammer) with an optimum offset of 9 m and a 24-bit seismograph to record the data.

The DH test measures the time necessary to the *P* and *S* waves to travel from the seismic source to the geophones located into the borehole. The schema adopted for the DH test are composed by 4 geophones placed in an horizontal plane at 45° one from the other and 1 located in the vertical plane (Di Fiore et al. 2020). The arrival times of *P* and *S* waves plotted against the depth made possible to outline the dromocrone and calculate the velocities of *P* and *S* waves for each slope changes. This test reached a depth of − 30 m (Fig. 5).

Table 2 Thickness and lithology of boreholes drilled in the present study

Drill-hole	Elevation (m, a.s.l)	Thickness (m)	Lithology
S1	2	3	Light brown sandy clay
		27	Organic-rich gray sandy silts with wood and peat levels
S2	1	4	Light brown sandy clay
		16	Clayey silt and silty sand with fin to silty sands
		20	Sandy deposits with gravelly bodies
		15	Organic-rich gray sandy silts with wood and peat levels
S3	4	8	Light brown sandy clay
		3	Organic-rich gray sandy silts with wood and peat levels
		5	Gray clayey sand with brackish to nearshore molluscs
		14	Organic-rich gray sandy silts with wood and peat levels
		2	Grayish cinerite associated with black scoriae and molten lava, with different degrees of diagenesis
S4	4	8	Light brown sandy clay
		4	Gray silt and clayey silts
		6	Gray clayey sand with brackish to nearshore molluscs
		4	Organic-rich gray sandy silts with wood and peat levels
		28	Grayish cinerite associated with black scoriae and molten lava, with different degrees of diagenesis

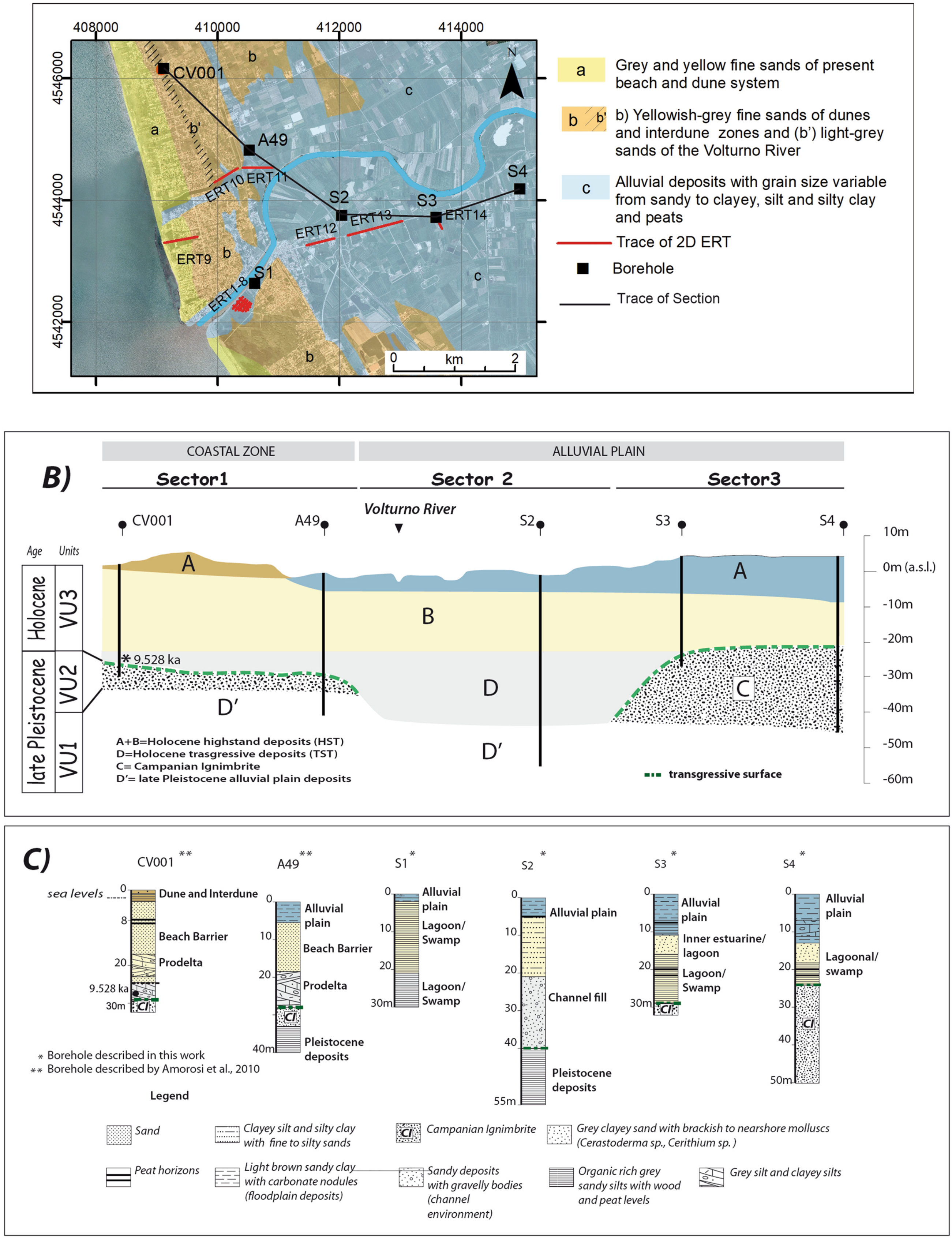
408000
410000
412000
414000
4546000
4544000
4542000
CV001
A49
S1
S2
S3
S4
ERT10
ERT11
ERT12
ERT13
ERT14
ERT9
ERT1-8
a
b
b'
c
N
0 km 2
a Grey and yellow fine sands of present beach and dune system
b b' b) Yellowish-grey fine sands of dunes and interdune zones and (b') light-grey sands of the Volturno River
c Alluvial deposits with grain size variable from sandy to clayey, silt and silty clay and peats
Trace of 2D ERT
Borehole
Trace of Section
B)
COASTAL ZONE
ALLUVIAL PLAIN
Sector1
Sector 2
Sector3
Volturno River
Age
Units
Holocene
late Pleistocene
VU3
VU2
VU1
A
B
C
D
D′
* 9.528 ka
10m
0m (a.s.l.)
-10m
-20m
-30m
-40m
-50m
-60m
A+B=Holocene highstand deposits (HST)
D=Holocene trasgressive deposits (TST)
C= Campanian Ignimbrite
D′= late Pleistocene alluvial plain deposits
transgressive surface
C)
CV001 **
A49 **
S1 *
S2 *
S3 *
S4 *
sea levels
Dune and Interdune
Beach Barrier
Prodelta
9.528 ka
30m
Alluvial plain
Pleistocene deposits
40m
Lagoon/ Swamp
30m
Channel fill
55m
Inner estuarine/ lagoon
Lagoonal/ swamp
50m
CI
* Borehole described in this work
** Borehole described by Amorosi et al., 2010
Legend
Sand
Clayey silt and silty clay with fine to silty sands
Campanian Ignimbrite
Grey clayey sand with brackish to nearshore molluscs (Cerastoderma sp., Cerithium sp.)
Peat horizons
Light brown sandy clay with carbonate nodules (floodplain deposits)
Sandy deposits with gravelly bodies (channel environment)
Organic rich grey sandy silts with wood and peat levels
Grey silt and clayey silts

◂**Fig. 6** **A** Geological sketch map of VCP. **B** Lithostratigraphic scheme of VCP reconstructed from boreholes. The tick marks show the location of the boreholes. **C** Stratigraphy of six boreholes representative of the subsurface geology. The single star indicates the boreholes made for the present work, while the double star signs the boreholes recover from scientific literature. The colors filling the boreholes indicate a connection with the layers (A, B, C, D, D') and sectors (sector1, sector 2, sector 3) drawn in the lithostratigraphic scheme (**B**)

The recorded data were stacked to improve signal-to-noise ratio, and the SurfSeis software (Park et al. 1999) was used to process the 1-D velocity profile of V_s. The MASW reached a penetration depth of − 70 m and − 90 m (Fig. 5).

Boreholes

In the coastal plains, boreholes are the only direct investigation tool of the subsurface geology that is useful for the geological interpretation of the resistivity layers shown by 2D-ERT and 3D-ERT profiles. At this aim, we used the geological data retrieved from the boreholes S1, S2, S3, S4, realized for this work (Table 2) and from the A49 (Caserta Provincial Territorial Plan, 2005) and CV001 (Amorosi et al. 2012) closer to the coastal zone (Fig. 2).

Furthermore, these boreholes together with those available from the scientific literature supported the reconstruction of palaeomorphology after the deposition of CI. This latter plays a key role in the hydrogeology; in fact, its presence can determine, as a relative impermeability, the separation between the main and shallow aquifers. The top of CI was generated with two steps: (i) the depth of the upper portion of CI, retrieved in 40 drill-holes (Pagliuca; 2009), was corrected according to the global mean sea level characterizing the MIS3.1 (Waelbroek et al. 2002) and the subsidence rate of 0.3 cm/yr defined for the last 50 ka by Ferranti et al. (2006); (ii) these values were interpolated with the inverse distance weighted method (Wu et al. 2021; Pando and Flor-Blanco 2022).

Data interpretation

The integration of *2D-ERT* and *3D-ERT, MASW, DH,* boreholes, information from *Geological Map (sheet 171 "Gaeta",* 1968*)* allowed to improve the knowledge on the saltwater intrusion at VCP.

Stratigraphic schema of Volturno Coastal Plain

The VCP is characterized by three informal stratigraphic units (VU1, VU2, VU3) focused on the lithological features of deposits (Fig. 6).

Moving landward from the present coastline the *VU3* marks the transition from the dune system (*layer A, sector 1*) to the alluvial plain (*layer A, sector 2, 3*) and from the beach barrier (layer B, sector 1) to the lagoon-swamp zones (*layer B, sector 2)* and to alluvial plain (*layer B, sector 3)* (Fig. 6a, b).

The *VU2* is made up of CI deposits (*layer C, sectors 1 and 3*) that is replaced by coarse alluvial deposits in the area of the Volturno River course (*layer D, sectors 3*) and is overlaid by prodelta clayey deposits close to the coast (*layer D, sectors 1*).

The CI is a relative impermeable placed at about − 20 m depth (measure referred to the present mean sea level) in the zones close to shoreline and of − 15 m at about 10 km landward (Fig. 7). These deposits are laterally discontinuous and have a thickness varying from 5 m, in the valley axes, to 40 m at the foot of slopes that border the plain, and it is often lacking in the area close to the Volturno River (Fig. 7).

The *VU1* is made up of Late Pleistocene marine-alluvial deposits (*layer D', sectors 1–3)*. This layer is overlaid by the Campanian Ignimbrite (C) and by Holocene deposits (D) where CI is lacking (sector 2, Fig. 6a).

2D-ERT analysis

The resistivity (ρ) made it possible to identify areas of the VCP saturated with brackish and salt water.

ERTs 1–8—The interpretation of these profiles was supported by the stratigraphy of borehole *S1*(Fig. 6), only the most representative profile was described. *It* has ρ ranging between 0.4 and 15 Ωm and show three main resistivity layers (Fig. 8). The *layer A* has ρ ranging from 8 to 15 Ωm up to 2.5 m depth; it may correspond with sandy clay and sandy silt of alluvial and lagoon-swamp environment, respectively (Fig. 6a, b, c). The *layer B,* located between 4 and 18 m depth, has a low ρ raging between 0.01 and 2 Ωm (Fig. 8); it well match with sandy silt deposits of lagoon-swamp environment seawater saturated (Fig. 6a, b, c). The *layer D* (depth: > 18 m) has ρ varying from 3 to 8 Ωm (Fig. 8); it could be characterized by less porous deposits of layer B seawater saturated.

ERT 9—The analysis of this profile was supported by the borehole CV001 (Fig. 6a, b, c); it shows three layers characterized by ρ ranging from 0.07 up to 35 Ωm (Fig. 8).

The *layer A* encompasses the first 10 m depth, it shows $\rho > 10$ Ωm and a wedge shape geometry slightly dipping seaward, it extends from the shoreline up to 100 m landward. The lateral continuity of *this layer* is interrupted by a small zone, with lower ρ, placed from 100 to 275 m landward (Fig. 8). The wedge shaped of *layer A* and the small zones with lower resistivity, probably coincides with sand of present day beach deposits, while the inner sector, characterized by lateral continuity, may characterized by clayey silt and

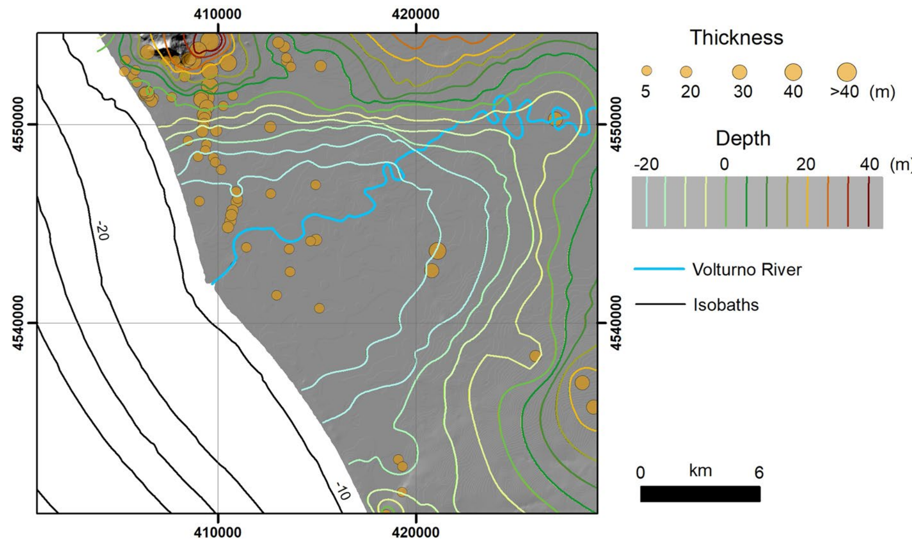

Fig. 7 Thickness (orange dots) and depth (lines from light cyan to brown) of Campanian Ignimbrite are displayed; the depth is referred to the present mean sea level. Data are overlaid to a gray tones shaded relief of VCP. The isobaths were derived from the Nautic map “Da Capo Circeo a Ischia e Isole Pontine” of Hydrographic Institute of Marina Militare Italiana

fine to medium sands of dune and interdune environment (Fig. 6a, b, c). Downward, a zone with lower ρ (< 2 Ωm), extended from – 10 m to – 30 m (*layer B*), contains several lenticular thick bodies with ρ > 10 Ωm. This *layer* is characterized a sequence of sand (beach barrier environment) and silt and clayey silt deposits (prodelta environment) seawater saturated confined at depth of about 30 m by the *layer C* (Fig. 6) with ρ > 30 Ωm (CI) (Fig. 8). The presence of these deposits is also corroborated by the changes of share wave velocity (V_s) recorded by the *MASW_01* end *MASW_02* (figs. 5 and 8).

ERT 10—This profile was interpreted with the support of borehole A49 (Fig. 6a, b, c). It has a layer *A* about 10 m thick. The continuity of this layer, showing ρ between 8 and 30 Ωm, is interrupted by two zones, located from 15 to 125 m and from 225 to 300 m, characterized by ρ ranging from 6 to 10 Ωm (Fig. 8). It could consist of pedogenized silt and clayey silt of alluvial environment and fine to medium sands deposits of beach barrier environment (Fig. 6a, b, c). The underlying layer *B*, with a bottom located between – 25 m and – 40 m depth, has ρ < 2 Ωm (Fig. 8). This features could correspond with a sequence of silt and clayey silt deposits of prodelta environment seawater saturated containing lenticular structures with higher resistivity (Fig. 8). The *layer D* reaches about -90 m; it is characterized by lenses-shaped bodies with high ρ (15–35 Ωm). At bottom of this layer, it is possible to observe a zone (layer D’) with ρ comparable to that typify the layer B. It could correspond with a saltwater lens connected with the layer B (Fig. 8).

The *ERT 11*—This profile was interpreted with the support of borehole *A49* (Fig. 6a, b, c). It consists of a top *layer A* with ρ between 6 and 15 Ωm along the first 100 m; it reaches – 10 m depth and pinches out landward reaching about – 5 m. This layer may consist of pedogenized sandy clay of alluvial plain environment. The *layer B* shows a sub-parallel geometry with ρ < 3 Ωm; it may consist of sand deposits (beach barrier environment) silt and clayey silts deposits of prodelta environment saltwater saturated. The lowest layer D shows a slightly increases of ρ (3–6 Ωm) (Fig. 8). This *layer* could correspond to the Pleistocene sandy silt with peat deposits saltwater saturated (Fig. 6a, b, c).

ERTs 12 and *13*—The interpretation is supported by the borehole *S2* (Fig. 6a, b, c). These profiles point out a top *layer A* with ρ ranging from 10 to 25 Ωm extended from field plain to about – 15 m depth. It could be made up of sandy clay of alluvial environment (Fig. 6a, b, c). The *layer B,* typified by ρ varying from 1.5 to 4 Ωm, is probably made up of clayey silt and silty clay with fine to silty sand deposits of alluvial plain environment (Fig. 6a, b, c) salty-brackish water saturated and contains lens-shaped bodies with lower resistivity. The lowest *layer C,* located at a depth of about 40 m, shows ρ > 15 Ωm and may correspond to the CI deposits. The latter, in profile 13, is locally interrupted by a body with lower ρ (2–4 Ωm) located along the profile between 160 and 290 m (Fig. 8).

The *ERT 14*—The interpretation is supported by the borehole *S3* (Fig. 6a, b, c). This profile consists of a top *layer* A characterized by ρ higher than 10 Ωm (Fig. 8). It may correspond with the sandy clay with peats layer of alluvial plain environment (Fig. 6a, b, c). At a depth of – 10 m, the intermediate *layer B,* with ρ ranging between 4 and 10 Ωm (Fig. 8), shows a sub-parallel geometry which continues downward for about 20 m with a sequence of gray sandy silt and clayey sand of lagoon-swamp environment salty-brackish water saturated. The lowest *layer C* shows an increases of ρ ranging from 10 and 15 Ωm (CI deposit) (Fig. 8).

3D-ERT models

The 3D resistivity survey made possible to monitor the saltwater intrusion up to − 20 m in both spatial and temporal domains. The horizontal slices of four resistivity seasonal models point out small variations of ρ: (a) 4.36–31.2 Ωm; (b) 4.66–30.36 Ωm; (c) 7.45–32.7 Ωm; (d) 2.97–35 Ωm. In the spring period, the slices show ρ ranging from 10 to 15 Ωm in the first 6 m depth, particularly the slices of May 2014 pointed out a resistivity of 15 Ωm at the 2 m depth, while in 2015 this value is recorded at about 6 m depth. The ρ increase to 25–30 Ωm is at a depth of 18 m to return successively at lower values (5–15 Ωm) at depth of about 20 m (Fig. 9). In the autumn, all slices show higher resistivity than in the springer period and particularly, ρ ranging between 10 and 15 Ωm and between 15 and 30 Ωm at 2 and 6 m depth, respectively (Fig. 9).

The bottom layer (at a depth of about 20 m) is characterized by discontinuous bodies with resistivity values comparable with those of layer B passing laterally to bodies with lower resistivity. The topmost layer shows low resistivity for largest zones with (for the first 4 m depth) that may correspond with more relative permeable lithology saturated by a surficial aquifer. On May, the topmost layer preserves the shape of geological bodies but appears less resistive; it is probably due to the rise of groundwater after the recharge of the springer period. The 3D-ERT better discriminated the resistivity variations in the first 6 m depth; they do not show the presence of saltwater in this zone.

Multichannel analysis of surface waves and down-hole tests

The analysis of *MASW-01* points out a $V_s < 200$ m/s for the first 20 m depth identified as *layer A* in the ERT 9. At about 40–50 m depth, the V_s close to 400 m/s supports the interpretation of *layer C* as the upper part of CI deposits (Guadagno et al. 1995). Similarly, the MASW-*02* also highlights a velocity changes at about 70 m depth evidencing a slightly deepening of CI deposits (Fig. 5).

The DH data analysis evidenced two important results: (i) the presence of a saturated layer for a depth greater than − 7 m as evidenced by the distribution of compressional wave velocity ($V_p > 1200$ m/s—Zelt et al. 2006); (ii) the presence of thin denser layers, located at about − 10 m and − 20 m depth, testified by the increase of shear wave velocity (V_s) and of the bulk density (Fig. 5). The DHs aided to corroborate the soil saturation evidenced by the ERTs even though these measurements were not made at same times. This was possible for the slow response of groundwater systems to weather variability or climate change (Ducci and Polemio 2018). A campaign conducted in 2015 showed for the main aquifer almost the same levels as in 2003, favored by stable rainfall (Ducci and Polemio 2018).

The density of this layers is consistent with a different diagenesis (i.e., variation in degrees of consolidation, in porosity, in textural and mineralogical characteristics) observed in the late Pleistocene-Holocene clayey units in several Mediterranean coastal plains. The higher density could be related to an over-consolidation process of sediment caused by the vertical fluctuations of the water table (Corazza et al. 1999; Bozzano et al. 2000). Such vertical fluctuations seem to be induced, in the lower parts of the river systems and close to the coastline, by the quasi-still stand of the sea level at the time of the Maximum Food Surface (see Posamentier and Allen 1999). The consolidation processes could be also due to the original depositional environments and to the consequent climatic changes (Rohrlich et al. 1995; Bonardi et al. 2004; Mancini et al. 2013; Pepe et al. 2015).

Discussion and conclusive remarks

The present research highlighted the key role of ERT surveys to delineate the spatial extent of saltwater intrusion in coastal plains. The integration into a Geographic Information System of MASWs, DHs, borehole stratigraphies and geological maps made it possible to draw a stratigraphic schema of Volturno Coastal Plain useful for the interpretation of ERT sections. This schema together with the difference in resistivity, that characterizes fresh (10–100 Ω) and saltwater (0.2 Ω) (Moulds et al. 2023 and reference therein), allowed us to recognize the distance reached by the saline wedge from the coastal belt.

The subsurface was found to consist of five resistivity layers labelled A, B, C, D and D', the layer B is saltwater saturated and the layer D is brackish water saturated. The lateral discontinuous of all layer favors the vertical migration of groundwater that is avoided only in the zones characterized by a continuity of *layer C* (Campanian Ignimbrite).

More important is the presence of thin denser layers at -10 and -20 m depth highlighted by the comparison of V_s, V_p and *bulk modulus* of DHs tests (Fig. 5). They represent a type of relative impermeable that makes more difficult the vertical groundwater seepage between the shallow local aquifer, characterizing the *layer A,* and the main aquifer of *layer B*.

Furthermore, the discontinuity of the CI makes this deposit a non-perfect aquiclude and exposes the deep aquifer to possible contamination by surface aquifers.

The 2D ERTs evidenced two zones water saturated, also pointed out by the DHs (Fig. 5), with different salinity.

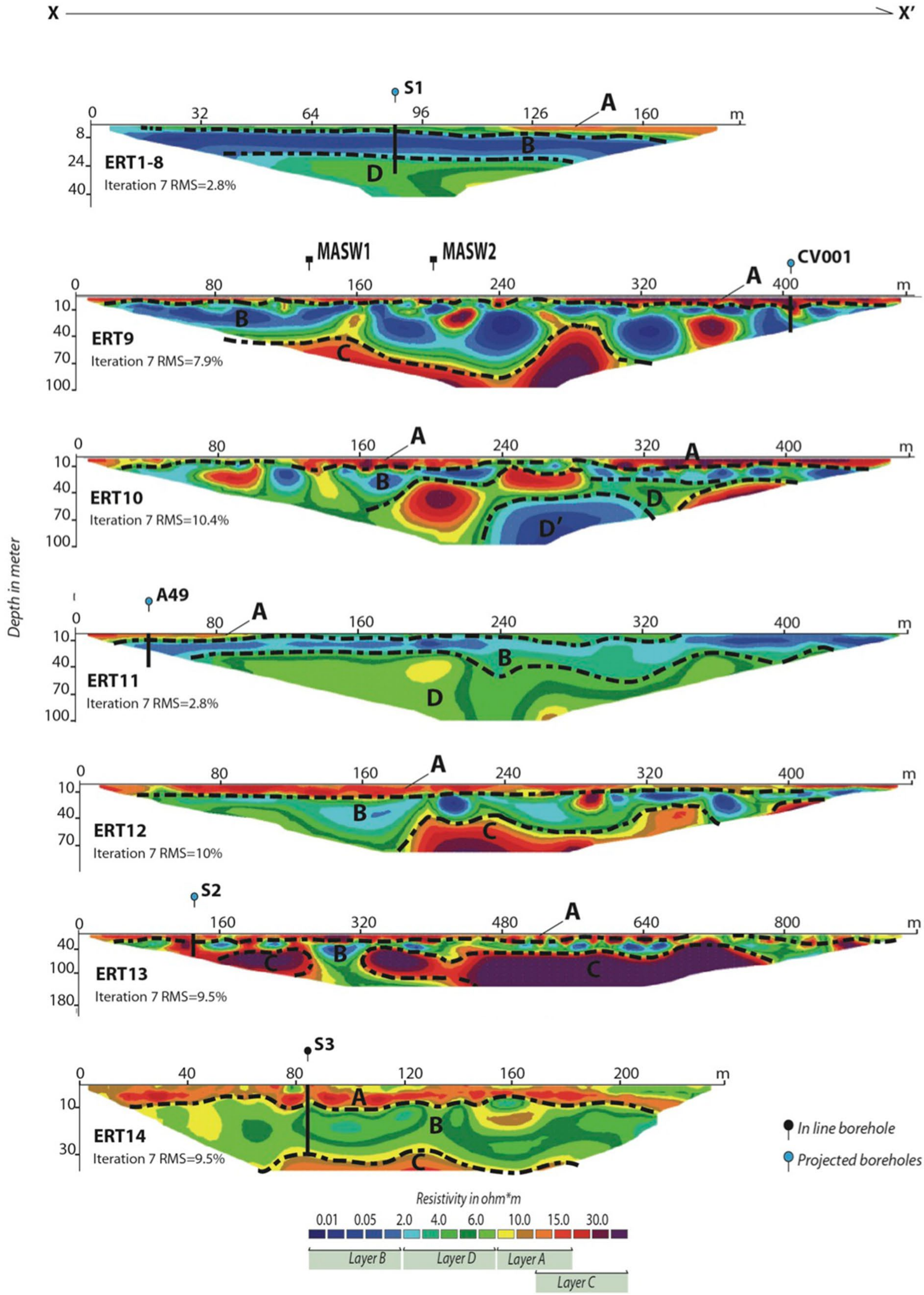
X
X′
S1
A
B
D
ERT1-8
Iteration 7 RMS=2.8%
MASW1
MASW2
CV001
ERT9
Iteration 7 RMS=7.9%
C
ERT10
Iteration 7 RMS=10.4%
D′
A49
ERT11
Iteration 7 RMS=2.8%
ERT12
Iteration 7 RMS=10%
S2
ERT13
Iteration 7 RMS=9.5%
S3
ERT14
Iteration 7 RMS=9.5%
Depth in meter
m
In line borehole
Projected boreholes
Resistivity in ohm*m
0.01 0.05 2.0 4.0 6.0 10.0 15.0 30.0
Layer B
Layer D
Layer A
Layer C

◂**Fig. 8** Electrical Resistivity Tomography sections realized in the VCP (the location is reported in Fig. 6). The dashed lines identify the boundaries between layers characterized by the same range of resistivity values, while the capital letters refer to the geological interpretation reported in detail along the text.

The first zone, extended from the coast up to 1.7 km inland (Fig. 10), is characterized by a very low resistivity (≤ 2 Ωm) that testifies the presence of seawater from − 4 m up to about − 30 m depth. The second zone, extended from 1.7 to 3 km inland, is characterized by a resistivity ranging from 2 to 5 Ωm that indicates the presence of salty-brackish water within a depth range from − 10 m to − 30 m (Fig. 10). The latter may be due to the mixing of salt and fresh water (salt wedge transition zone) and/or brackish water of the Volturno River that feed the aquifer (Corniello et al. 2010).

The 3D-ERT better discriminated the resistivity variations in the first 6 m depth and gave 2D shape of geological bodies. The resistivity values characterizing the first meters of *layer A* exclude the saltwater contamination in this zone as also confirmed by the groundwater samples from elm xylem and soil profiles which showed negative $\delta^{18}O$ values, indicating the continental or meteoric nature of the groundwater (Esposito 2017, PhD Thesis).

This work shows the full potential of 2D ERTs and 3d ERT to study saltwater intrusion despite the absence of hydro-physical parameters measurements in wells suitable to validate the ERT interpretation (Folorunso et al. 2021). Anyway, the availability of DHs, to corroborate the saturation of ERT layers, together with borehole stratigraphies allowed us to recognize the presence of salt and brackish water layers.

Future analyses will be focused on some aspects that still need more investigation such as the freshwater contamination both at distances greater than 3 km inland and at greater distances from the Volturno River and others channels. Furthermore, the presence of paleo-channels, which may represent a priority passages for saltwater intrusion, as also the

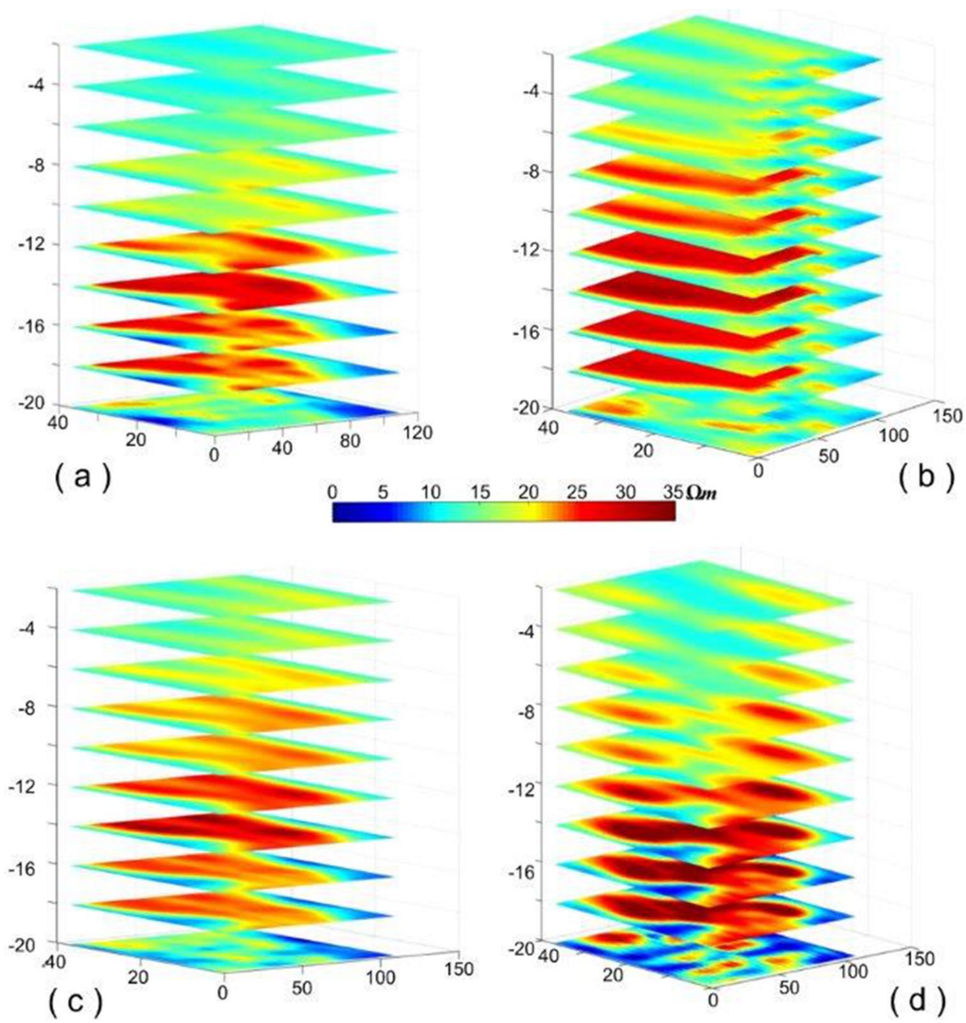

Fig. 9 3D resistivity model of May (**a**) and October (**b**) 2013 and in May (**c**) and October (**d**) 2014

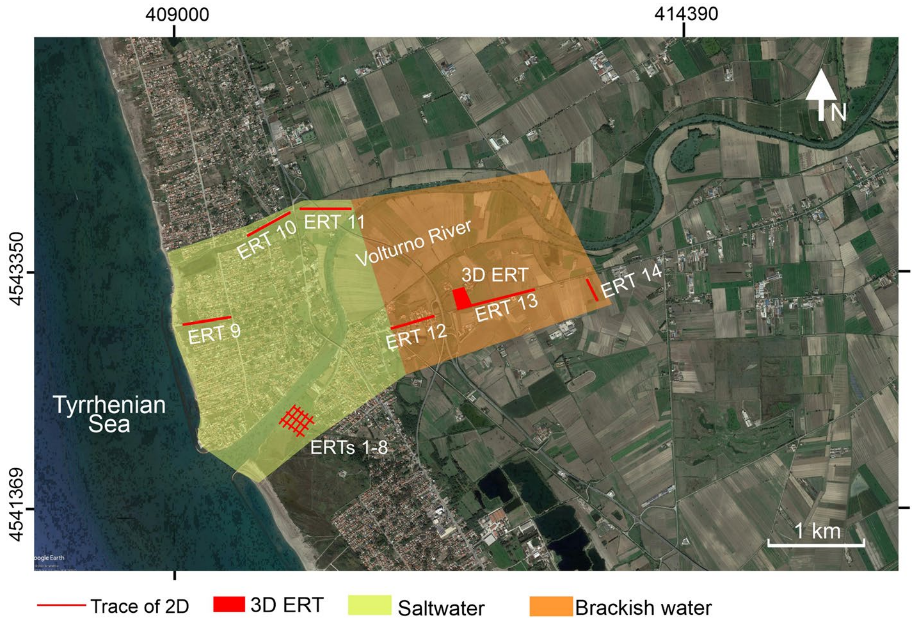

Fig. 10 The spatial distribution of saltwater and brackish water is shown

presence of lenses of fossil saltwater, which can contaminate surficial groundwater, will be investigated in the next future.

In the context of integrated coastal zone management, this information can help stakeholders gain insight into saltwater intrusion and provide some of the information needed to take the right actions (e.g., optimizing pumping rates, identifying the site for installing water wells) to preserve water quality status.

Acknowledgements We warmly thank Paolo Scotto di Vettimo and Michele Iavarone for supporting the geophysical survey. Grateful thanks go to anonymous reviewers, whose valuable suggestions greatly improved the first version of the manuscript. The availability of Chief Editor, prof. E. Drioli, is also warmly thanked.

Funding This study benefited from the contribution of I-AMICA Project (PON a3_00363) and RITMARE Project (MIUR, NRP 2011-2013) granted to Ines Alberico and Vincenzo Di Fiore. The funders had no role in study design, data collection and analysis, decision to publish or preparation of the manuscript.

Declarations

Conflict of interest The authors declare that they have no known competing financial interests or personal relationships that could have appeared to influence the work reported in this paper.

References

Alberico I, Iavarone R, Angrisani AC, Castiello A, Incarnato R, Barra R (2017) The potential vulnerability indices as tools for natural risk reduction. The Volturno coastal plain case study. J Coast Conserv 21:743. https://doi.org/10.1007/s11852-017-0534-4

Alberico I, Cavuoto G, Di Fiore V, Punzo M, Tarallo D, Pelosi N, Ferraro L, Marsella E (2018) Historical maps and satellite images as tools for shoreline variations and territorial changes assessment: the case study of Volturno Coastal Plain (Southern Italy). J Coast Conserv 22:919. https://doi.org/10.1007/s11852-017-0573-x

Alfarrah N, Walraevens K (2018) Groundwater overexploitation and seawater intrusion in coastal areas of arid and semi-arid regions. Water 10:143

Al-Halbouni D, Watson RA, Holohan EP, Meyer R, Polom U, Dos Santos FM, Comas X, Alrshdan H, Krawczyk CM, Dahm T (2021) Dynamics of hydrological and geomorphological processes in evaporite karst at the eastern Dead Sea: a multidisciplinary study. Hydrol Earth Syst Sci 25(6):3351–3395. https://doi.org/10.5194/hess-25-3351-2021

Al-Sayed EA, El-Quady G (2007) Evaluation of sea water intrusion using the electrical resistivity and transient electromagnetic survey: case study at Fan of Wadi Feiran, Sinai; Egypt. In: EGM 2007 international workshop, Italy

Amorosi A, Pacifico A, Rossi V, Ruberti D (2012) Late quaternary incision and deposition in an active volcanic setting: the Volturno Valley Fill, southern Italy. Sediment Geol 242:307–320

Antonellini M, Mollema P, Giambastiani B, Bishop K, Caruso L, Minchio A, Pellegrini L, Sabia M, Ulazzi E, Gabbianelli G (2008) Salt water intrusion in the coastal aquifer of the southern Po Plain, Italy. Hydrogeol J. https://doi.org/10.1007/s10040-008-0319-9

Aprile F, Ortolani F (1978) Nuovi dati sulla struttura profonda della piana campana a sud est del fiume Volturno. Boll Soc Geol Ital 97:591–608

Barra D, Bonaduce G, Brancaccio L, Cinque A, Ortolani F, Pagliuca S, Russo F (1989) Evoluzione geologica olocenica della piana costiera del fiume Sarno (Campania). Mem Soc Geol It 42:255–267

Bhattachan A, Emanuel RE, Ardón M, Bernhardt ES, Anderson SM, Stillwagon MG, Ury EA, BenDor TK, Wright PJ (2018) Evaluating the effects of land-use change and future climate change on vulnerability of coastal landscapes to saltwater intrusion. Elem Sci Anth 6:62. https://doi.org/10.1525/elementa.316

Bonardi M, Tosi L, Rizzetto F, Brancolini G, Baradello L (2004) Effects of climate changes on the late Pleistocene and Holocene sediments of the Venice Lagoon, Italy. J Coast Res SI 39:279–284

Boyd R, Darlymple RW, Zaitlin BA (2006) Estuarine and incised-valley faciesmodels. In: Posamentier HW, Walker RG (eds) Facies models revis-ited, vol 84. SEPM Society of Economic Paleontologists and Mineralogists, Tulsa, pp 171–235

Bozzano F, Andreucci A, Gaeta M, Salucci R (2000) A geological model of the buried Tiber River valley beneath the historical centre of Rome. Bull Eng Geol Env 59:1–21. https://doi.org/10.1007/s100640000051

Bruno PP, Di Fiore V, Ventura G (2000) Seismic study of the '41st parallel' fault system offshore the Campanian–Latial continental margin, Italy. Tectonophysics 324(1):37–55. https://doi.org/10.1016/S0040-1951(00)00114-1

Busico G, Cuoco E, Kazakis N, Colombani N, Mastrocicco M, Tedesco D, Voudouris K (2018) Multivariate statistical analysis to characterize/discriminate between anthropogenic and geogenic trace elements occurrence in the Campania Plain, Southern Italy. Environ Pollut 234:260–269. https://doi.org/10.1016/j.envpol.2017.11.053

Caserta Provinciali Territorial Plan (2012) http://trasparenza.provincia.caserta.it:81/web/amministrazione-trasparente/pianificazione-e-governo-del-territorio

Castel Volturno Municipal Urban Plan (2021) https://www.puccastelvolturno.it/index.php/contenuti

Celico F, Naclerio G, Bucci A, Nerone V, Capuano P, Carcione M, Allocca V, Celico P (2010) Influence of pyroclastic soil on epikarst formation: a test study in southern Italy. Terra Nova 22(2):110–115. https://doi.org/10.1111/j.1365-3121.2009.00923.x

Chabaane A, Redhaounia B, Gabtni H, Adnen Amiri A (2018) Contribution of geophysics to geometric characterization of freshwater–saltwater interface in the Maâmoura region (NE Tunisia). Euro-Mediterr J Environ Integr 3:26. https://doi.org/10.1007/s41207-018-0068-7

Chitea F, Georgescu P, Ioane D (2011) Geophysical detection of marine intrusion in black sea coastal areas (Romania) using VES and ERT data. Geo-Eco-Marina 17:95–102

Cianflone G, Cavuoto G, Punzo M, Dominici R, Sonnino M, Di Fiore V, Pellosi N, Tarallo D, Lirer F, Marsella E (2018) Late quaternary stratigraphic setting of the Sibari Plain (southern Italy): hydrogeological implications. Mar Pet Geol 97:422–436. https://doi.org/10.1016/j.marpetgeo.2018.07.027

Cinque A, Alinaghi HH, Laureti L, Russo F (1987) Osservazioni preliminari sull'evoluzione geomorfologica della Piana del Sarno (Campania, Appennino meridionale). Geogr Fis Dinam Quat 10:161–174

Cinque A, Aucelli PPC, Brancaccio L, Mele R, Milia A, Robustelli G, Romano P, Russo F, Russo M, Santangelo N, Sgambati D (1997) Volcanism, tectonics and recent geomorphological change in the bay of Napoli, I.A.G. In: IV international conference on geomorphology, supplementi di geografia fisica e dinamica quaternaria III (T 2), pp 123–141

Cinque A, Robustelli G, Russo M (2000) The consequences of pyroclastic follout on the dynamics of mountain catchments: geomorphic events in the Rivo d'Arco basin (sorrento Peninsula, Italy) after the Plinian eruption of Vesuvius in 79 A.D. Geogr Fis Din Quat 23:117–129

Corazza A, Lanzini M, Rosa C, Salucci R (1999) Caratteri stratigrafici, idrogeologici e geotecnici delle alluvioni tiberine nel settore del centro storico di Roma. Il Quaternario 12:215–235

Corniello A, Ducci D (2014) Hydrogeochemical characterization of the main aquifer of the "Litorale Domizio-Agro Aversano NIPS" (Campania—southern Italy). J Geochem Explor 137:1–10. https://doi.org/10.1016/j.gexplo.2013.10.016

Corniello A, Ducci D, Trifuoggi M, Rotella M, Ruggieri G (2010) Hydrogeology and hydrogeochemistry of the plain between Mt. Massico and river Volturno (Campania region, Italy). Ital J Eng Geol Environ 1:51–64. https://doi.org/10.4408/IJEGE.2010-01.O-04

Dalrymple RW, Leckie DA, Tillman RW (2006) Incised valleys in time and space, vol 85. SEPM (Society of Economic Paleontologists and Mineralogists) Sp. Publ, Tulsa, p 348

De Vivo B, Rolandi G, Gans PB, Calvert A, Bohrson WA, Spera FJ, Belkin HE (2001) New constraints on the pyroclastic eruptive history of the Campanian volcanic Plain (Italy). Mineral Petrol 73:47–65. https://doi.org/10.1007/s007100170010

Di Fiore V, Cavuoto G, Tarallo D, Punzo M, Evangelista L (2015) Multichannel analysis of surface waves and down-hole tests in the archeological "Palatine Hill" Area (Rome, Italy): evaluation and influence of 2D effects on the shear wave velocity. Surv Geophys. https://doi.org/10.1007/s10712-015-9350-2

Di Fiore V, Albarello D, Cavuoto G, De Franco R, Pelosi N, Punzo M, Tarallo D (2020) Downhole seismic wave velocity uncertainty evaluation by theoretical simulation and experimental data acquired during the seismic microzonation of Central Italy. Soil Dyn Earthq Eng 138:106319. https://doi.org/10.1016/j.soildyn.2020.106319

Doll P (2009) Vulnerability to the impact of climate change on renewable groundwater resources: a global-scale assessment. Environ Res Lett 4:12. https://doi.org/10.1088/1748-9326/4/3/035006

Doyle TW, O'Nei CP, Melder MP (2007) Tidal freshwater swamps of the southeastern United States: effects of land use, hurricanes, sea-level rise, and climate change. In: Conner WH, Doyle TW, Krauss KW (eds) Ecology of tidal freshwater forested wetlands of the southeastern United States. Springer, Dordrecht, pp 1–28. https://doi.org/10.1007/978-1-4020-5095-4_1

Ducci D, Polemio M (2018) Quantitative impact of climate variations on groundwater in southern Italy. In: Calvache ML, Duque C, Pulido-Velazquez D (eds) Groundwater and global change in the western Mediterranean area. Springer, Heidelberg, pp 101–108. https://doi.org/10.1007/978-3-319-69356-9_12

Ducci D, Della Morte R, Mottola A, Onorati G, Pugliano G (2020) Evaluating upward trends in groundwater nitrate concentrations: an example in an alluvial plain of the Campania region (Southern Italy). Environ Earth Sci 79:319. https://doi.org/10.1007/s12665-020-09062-8

Ekwok SE, Ben UC, Eldosouky AM, Qaysi S, Abdelrahman K, Akpan AE, Andráš P (2022) Towards understanding the extent of saltwater incursion into the coastal aquifers of Akwa Ibom State, Southern Nigeria using 2D ERT. J King Saud Univ Sci. https://doi.org/10.1016/j.jksus.2022.102371

Esposito R (2017) Application of a multidisciplinary approach to investigate on a possible secondary soil salinization, due to seawater intrusiondynamics, at the Volturno river mouth. PhD Thesis https://dspace.unitus.it/bitstream/2067/3092/1/resposito_tesid.pdf

Ferranti L, Antonioli F, Mauz B, Amorosi A, Dai Pra G, Mastronuzzi G, Monaco C, Orrù P, Pappalardo M, Radtke U, Renda P, Romano P, Sansò P, Verrubbi V (2006) Markers of the last interglacial sea level high stand along the coast of Italy: tectonic implications. Quat Int 145–146:30–54

Ferraro L, Giordano L, Bonomo S, Cascella A, Di Martino G, Innangi S, Gherardi S, Tamburrino S, Alberico I, Budillon F, Di Fiore V, Punzo M, Tarallo D, Anzalone E, Capodanno M, Cavuoto G, Evangelista L, Ferraro R, Iavarone M, Iengo A, Lirer F, Marsella E., Migliaccio R, Molisso F, Pelosi N, Rumolo P, Scotto di Vettimo P, Tonielli T, Vallefuoco M. (2017) Monitoraggio integrato di un'area marino-costiera: la foce del fiume Volturno (Mar Tirreno centrale). Quad Geofis 146. ISSN 1590-2595. pp 4–57

Folorunso AF (2021) Mapping a spatial salinity flow from seawater to groundwater using electrical resistivity topography techniques. Sci Afr 13:e00957. https://doi.org/10.1016/j.sciaf.2021.e00957

Gemail K, Samir A, Oelsner C, Mousa SE, Ibrahim S (2004) Study of saltwater intrusion using 1D, 2D and 3D resistivity surveys in the coastal depressions at the eastern part of Matruh area. Egypt near Surf Geophys 2:103–109

Giaccio B, Hajdas I, Isaia R, Deino A, Nomade S (2017) High-precision ^{14}C and ^{40}Ar/^{39}Ar dating of the Campanian Ignimbrite (Y-5) reconciles the time-scales of climatic-cultural processes at 40 ka. Sci Rep 7(158):211–234. https://doi.org/10.1038/srep45940

Giménez-Forcada E (2014) Space/time development of seawater intrusion: a study case in Vinaroz coastal plain (eastern Spain) using HFE-diagram, and spatial distribution of hydrochemical facies. J Hydrol 517:617–627. https://doi.org/10.1016/j.jhydrol.2014.05.056

Guadagno FM, Mele R, Nunziata C (1995) Shear wave velocities of Campanian tuffs (Southern Italy). In: Proceedings of 1st meeting of EEGS European section, Torino, p 8. https://www.researchgate.net/publication/301472232_Shear_Wave_Velocities_of_Campanian_Tuffs_Southern_Italy

Herbert ER, Boon P, Amy JB, Scott CN, Rima BF, Ardón M, Hopfensperger KN, Lamers LPM, Gell PA (2015) A global perspective on wetland salinization: ecological consequences of a growing threat to freshwater wetlands. Ecosphere. https://doi.org/10.1890/ES14-00534.1

Himi M, Stitou J, Rivero L, Salhi A, Tapias JC, Casas A (2004) Geophysical surveys for delineating salt water intrusion and fresh water resources in the Oued Laou coastal aquifer. In: Near surface—16th European meeting of environmental and engineering geophysics, abstracts volume, Switzerland

Iorio M, Capretto G, Petruccione E, Marsella E, Aiello G, Senatore MR (2014) Multi-proxy analysis in defining sedimentary processes in very recent prodelta deposits: the Northern Phlegraean offshore example (eastern Tyrrhenian margin). Rend Fis Acc Lincei 25:237–254. https://doi.org/10.1007/s12210-014-0303-3

Ippolito F, Ortolani F, Russo M (1973) Struttura marginale tirrenica dell'Appennino campano: reinterpretazione di dati di antiche ricerche di idrocarburi. Mem Soc Geol It 12:227–250

Italian geologiacal Survey (1968) Geological map of Italy, scale 1:100000, sheet no 171 Gaeta

Jasechko S, Perrone D, Seybold H, Fan Y, Kirchner JW (2020) Groundwater level observations in 250,000 coastal US wells reveal scope of potential seawater intrusion. Nat Commun 11:3229. https://doi.org/10.1038/s41467-020-17038-2

Ketabchi H, Mahmoodzadeh D, Ataie-Ashtiani B, Simmons CT (2016) Sea-level rise impacts on seawater intrusion in coastal aquifers: review and integration. J Hydrol 535:235–255. https://doi.org/10.1016/j.jhydrol.2016.01.083

Kim DG, Shin KH, Kim GB (2018) Suitability analysis of saline water intrusion monitoring wells near a waterway based on a numerical model and electric conductivity time series. Geosci J 22:807–824

Lasagna M, Mancini S, De Luca DA, Cravero M (2019) Piezometric levels in the Piedmont plain (NW Italy): trend and hydrodynamic behaviour of the shallow aquifer. Rend Online Soc Geol It 48:2–9. https://doi.org/10.3301/ROL.2019.30

Leduc C, Pulido-Bosch A, Remini B (2017) Anthropization of groundwater resources in the Mediterranean region: processes and challenges. Hydrogeol J 25:1529–1547. https://doi.org/10.1007/s10040-017-1572-6

Loke MH, Barker RD (1996a) Rapid least-squares inversion of apparent resistivity pseudosections by a quasi-Newton method. Geophys Prospect 44:131–152. https://doi.org/10.1111/j.1365-2478.1996.tb00142.x

Loke MH, Barker RD (1996b) Practical techniques for 3D resistivity surveys and data inversion. Geophys Prospect 44:499–523. https://doi.org/10.1111/j.1365-2478.1996.tb00162.x

Loke MH, Dahlin T, Rucker DF (2014) Smoothness-contrained timelapse inversion of data from 3D resistivity surveys. Near Surf Geophys 12:5–24

Mancini M, Moscatelli M, Stigliano F, Cavinato GP, Milli S, Pagliaroli A, Simionato M, Brancaleoni R, Cipolloni I, Coen G, Di Salvo C, Garbin F, Lanzo G, Napoleoni Q, Scarapazzi M, Storoni Ridolfi S, Vallone R (2013) The Upper Pleistocene-Holocene fluvial deposits of the Tiber River in Rome (Italy): lithofacies, geometries, stacking pattern and chronology. J Mediterr Earth Sci 5:95–101

Manda AK, Giuliano AS, Allen TR (2014) Influence of artificial channels on the source and extent of saline water intrusion in the wind tide dominated wetlands of the southern Albemarle estuarine system (USA). Environ Earth Sci 71(10):4409–4419. https://doi.org/10.1007/s12665-013-2834-9

Mariani M, Prato R (1988) I bacini Neogenici costieri del margine tirrenico: approccio sismico-stratigrafico. Mem Soc Geol Ital 41:519–531

Mastrocicco M, Colombani N (2021) The issue of groundwater salinization in coastal areas of the Mediterranean region: a review. Water 13:90. https://doi.org/10.3390/w13010090

Meyer R, Engesgaard P, Sonnenborg TO (2019) Origin and dynamics of saltwater intrusion in a regional aquifer: combining 3-D saltwater modelling with geophysical and geochemical data. Water Resour Res 55:1792–1813. https://doi.org/10.1029/2018WR023624

Milia A, Torrente M, Russo M, Zuppetta A (2003) Tectonics and crustal structure of the Campania continental margin: relationships with volcanism. Mineral Petrol 79:33–47. https://doi.org/10.1007/s00710-003-0005-5

Milia A, Torrente M, Massa B, Iannace P (2013) Progressive changes in rifting directions in the Campania margin (Italy): new constrains for the Tyrrhenian Sea opening. Glob Planet Change 109:3–17. https://doi.org/10.1016/j.gloplacha.2013.07.003

Moulds M, Gould I, Wright I, Webster D, Magnone D (2023) Use of electrical resistivity tomography to reveal the shallow freshwater–saline interface in the Fens coastal groundwater, eastern England (UK). Hydrogeol J 31:335–349. https://doi.org/10.1007/s10040-022-02586-2

Municipal Urban Plan of Castel Volturno (2008). https://www.puccastelvolturno.it/index.php/puc-elaborati

Muzzillo R, Zuffianò LE, Rizzo E, Canora F, Capozzoli L, Giampaolo V, De Giorgio G, Sdao F, Polemio M (2020) Seawater intrusion proneness and geophysical investigations in the Metaponto coastal plain (Basilicata, Italy). Water 13:53. https://doi.org/10.3390/w13010053

Ortolani F, Pagliuca S (1986) Relazioni tra struttura profonda ed aspetti morfologici e strutturali della fascia tirrenica dell'Appennino campano. Atti Riun Ann Gr Naz Geogr Fis e Geomorf, Amalfi (SA)

Pagliuca S (2009) Groundwater resources quality for irrigation in the lower Volturno plain (province of Naples and Caserta, Southern Italy). In: Annual international meeting project SWUP–MED, Adana, Turchia. https://www.yumpu.com/en/document/view/27753091/project-swup-med-beneficiary-4-a-cnr-isafom-first

Pando L, Flor-Blanco G, Liliana-Fúnez S (2022) Urban geology from a GIS-based geotechnical system: a case study in a medium-sized city (Oviedo, NW Spain). Environ Earth Sci 81:193. https://doi.org/10.1007/s12665-022-10287-y

Park CB, Miller RD, Xia J (1999) Multichannel analysis of surface waves. Geophysics 64(3):800–803

Pazdirek O, Blaha V (1996) Examples of resistivity imaging using ME-100 resistivity field acquisition system. In: EAGE 58th conference and technical exhibition extended abstracts, Amsterdam, P050

Pepe G, Coen G, Napoleoni Q, Pagliaroli A, Stigliano F, Mancini M, Lanzo G, Silvani S, Scarapazzi M (2015) SDMT testing for the estimation of in situ G decay curves in soft alluvial and organic soils. In: 3rd international conference on the flat dilatometer, June 14–16, 2015, Rome (Italy)

Posamentier HW, Allen GP (1999) Siliciclastic sequence stratigraphy: concepts and applications, vol 7. SEPM (Society for Sedimentary Geology), Tulsa. https://doi.org/10.2110/csp.99.07

Rohling E, Foster G, Grant K, Marino G, Roberts AP, Tamisiea ME, Williams FG (2014) Sea-level and deep-sea-temperature variability over the past 5.3 million years. Nature 508:477–482. https://doi.org/10.1038/nature13230

Rohrlich V, Wiseman G, Komornik A (1995) Overconsolidated clays from the Israeli Mediterranean coast and inner shore. Eng Geol 39(1–2):87–94

Romano P, Santo A, Voltaggio M (1994) L'evoluzione morfologica della pianura del Fiume Volturno (Campania) durante il tardo Quaternario (Pleistocene medio-superiore/Olocene). Il Quat 7(1):41–56

Ruberti D, Buffardi C, Sacchi M, Vigliotti M (2022) The late Pleistocene-Holocene changing morphology of the Volturno delta and coast (northern Campania, Italy): geological architecture and human influence. Quat Int 625:14–28

Sacchi M, Molisso F, Pacifico A, Vigliotti M, Sabbarese C, Ruberti D (2014) Late-Holocene to recent evolution of Lake Patria, South Italy: an example of a coastal lagoon within a Mediterranean delta system. Globary Planet Change 117:9–27

Salaj SS, Ramesh D, Suresh Babu DS, Kaliraj S (2018) Assessment of coastal change impact on seawater intrusion vulnerability in Kozhikode coastal stretch, South India using Geospatial technique. J Coast Sci 5(1):27–41

Sang-Ho L, Kyoung-Woong K, Ilwon K, Sang-Gyu L, Hak-Soo H (2002) Geochemical and geophysical monitoring of salinewater intrusion in Korean paddy fields. Environ Geochem Health 24(4):277–291

Scheidleger A, Grath J, Lindinger H (2004) Saltwater intrusion due to groundwater over-exploitation EEA inventory throughout Europe. In: Proceedings of 18th saltwater intrusion meeting, Cartagena, Spain, p 125

Schiavo M, Colombani N, Mastrocicco M (2023) Modeling stochastic saline groundwater occurrence in coastal aquifers. Water Res 235:119885. https://doi.org/10.1016/j.watres.2023.119885

Siddall M, Rohling EJ, Almogi-Labin A, Hemleben Ch, Meischner D, Schmelzer I, Smeed DA (2003) Sea-level fluctuations during the last glacial cycle. Nature 423:853–858

Singh AP, Gupta PK, Khandelwal M (2013) Prediction of sea water intrusion for mining activity in close precincts of sea shore. Springerplus 2:417

Tomaszkiewicz M, Abou Najm M, El-Fadel M (2014) Development of a groundwater quality index for seawater intrusion in coastal aquifers. Environ Model Softw 57:13–26

Tropeano M, Cilumbriello A, Grippa A, Sabatto L, Bianca M, Gallipoli MR, Mucciarelli M (2011) Stratigraphy of the subsurface of the metaponto plain vs a geophysical 3D view of the late Pleistocene incised-valleys (Basilicata, southern Italy). Rend Online Soc Geol Ital 17:187–193

Viezzoli A, Tosi L, Teatini P, Silvestri S (2010) Surface water-groundwater exchange in transitionale coastal environments by airbone electromagnetics: the Venice Lagoon example. Geophys Res Lett. https://doi.org/10.1029/2009GL041572

Waelbroeck C, Labeyrie L, Michel E, Duplessy JC, McManus JF, Lambeck K, Balbon E, Labracherie M (2002) Sea-level and deep water temperature changes derived from benthic foraminifera isotopic records. Quat Sci Rev 21:295–305

White E, Kaplan D (2017) Restore or retreat? Saltwater intrusion and water management in coastal wetlands. Ecosyst Health Sustain 3(1):1–18. https://doi.org/10.1002/ehs2.1258

Working Group of Water Protection Plan ex Basin Authority of North-Western Campania (2006) https://www.distrettoappenninomeridionale.it/index.php/elaborati-di-piano-menu/bacini-reg-nord-occidentali-bacino-reg-sarno-ex-adb-reg-campania-centrale-menu/piano-stralcio-per-la-tutela-del-suolo-e-delle-risorse-idriche-menu

Wu X, Liu G, Weng Z, Tian Y, Zhang Z, Li Y, Chen G (2021) Constructing 3D geological models based on large-scale geological maps. Open Geosci 13:851–866

Zahangeer MA, Carpenter-Boggs L, Mitra S, Haque MM, Halsey J, Rokonuzzaman M, Saha B, Moniruzzaman M (2012) Effect of salinity intrusion on food crops, livestock, and fish species at Kalapara coastal belt in Bangladesh. Hindawi J Food Qual 2017:23. https://doi.org/10.1155/2017/2045157

Zdruli P (2012) Land resources of the Mediterranean: status, pressures, trends and impacts on future regional development. Land Degrad. Develop. Published online in Wiley Online Library (wileyonlinelibrary.com). https://doi.org/10.1002/ldr.2150

Zelt AC, Azaria A, Levander A (2006) 3D seismic refraction traveltime tomography at a grounwater contamination site. Geophisics 58(9):1314–1323

Publisher's Note Springer Nature remains neutral with regard to jurisdictional claims in published maps and institutional affiliations.